JOURNAL OF Applied Polymer SCIENCE

Fabrication of Carbon Nanotubes/Polypyrrole/Carbon Nanotubes/ Melamine Foam for Supercapacitor

Feifei Liu, Gaoyi Han, Yunzhen Chang, Dongying Fu, Yanping Li, Miaoyu Li
Institute of Molecular Science, Key Laboratory of Chemical Biology and Molecular Engineering of Education Ministry of Shanxi University, Taiyuan 030006, People's Republic of China
Correspondence to: G. Han (E-mail: han_gaoyis@sxu.edu.cn)

ABSTRACT: The carbon nanotubes (CNTs) have been loaded on the melamine foam (MF) to form the composite (CNTs/MF) by dip-dry process, then polypyrrole (PPy) is coated on CNTs/MF (PPy/CNTs/MF) through chemical oxidation polymerization by using $FeCl_3 \cdot 6H_2O$ adsorbed on CNTs/MF as oxidant to polymerize the pyrrole vapor. Finally, CNTs are coated on the surface of PPy/CNTs/MF to increase the conductivity of the composite (CNTs/PPy/CNTs/MF) by dip-dry process again. The composites have been characterized by X-ray diffraction spectroscopy, scanning electron microscopy and electrochemical method. The results show that the structure of the composites has obvious influence on their capacitive properties. According to the galvanostatic charge/discharge test, the specific capacitance of CNTs/PPy/CNTs/MF is about 184 F g^{-1} based on the total mass of the composite and 262 F g^{-1} based on the mass of PPy (70.2 wt % in the composite) at the current density of 0.4 A g^{-1}, which is higher than that of PPy/CNTs/MF (120 F g^{-1} based on the total mass of the composite and 167 F g^{-1} based on the mass of the PPy). Furthermore, the capacitor assembled by CNTs/PPy/CNTs/MF shows excellent cyclic stability. The capacitance of the cell assembled by CNTs/PPy/CNTs/MF retains 96.3% over 450 scan cycles at scan rate of 20 mV s^{-1}, which is larger than that assembled by CNTs/PPy/MF (72.5%). © 2013 Wiley Periodicals, Inc. J. Appl. Polym. Sci. **2014**, *131*, 39779.

KEYWORDS: carbon nanotubes; composites; conducting polymers; supercapacitor

Received 5 February 2013; accepted 17 July 2013
DOI: 10.1002/app.39779

INTRODUCTION

The worldwide scientists and engineers have made various attempts in order to address the rapidly increasing global energy consumption coupled with the critical issue of climate change. Recently, there has been tremendous interest in flexible energy storage devices for applications in emerging flexible devices including portable wearable electronic devices,[1–3] solar cells,[4] flexible chemical batteries,[5–7] and flexible supercapacitors.[8,9] Among various energy storage devices, supercapacitors have been considered as one of the most promising candidates owing to their high power density, long cyclic lifetime, safety, and low environmental impact.[10–13] Various materials with high surface area and conductive polymers have been employed as electrodes in supercapacitors to achieve high capacitance. Kim et al.[14] have fabricated the polypyrrole (PPy)-based electrodes for energy storage applications using cellulose as substrate and the gravimetric charge capacity can reach 250 F g^{-1}. Jin et al.[15] have prepared the flexible composites of PPy/MnO_2/polypropylene fibrous membrane through the polymerization *in situ* vapor phase and the specific capacitance (C_{sc}) is calculated to be about 110 F g^{-1}. Recently, the composites of graphene and polyaniline nanofibers have bee fabricated by Wu et al.[16] through vacuum filtration and show large electrochemical capacitance of about 210 F g^{-1}. However, most of the reported C_{sc} is calculated according to the mass of active materials but not to the mass of the total electrodes. Furthermore, the proportion of the active material in the composites is only about 8–50%,[14–17] which makes the capacitance of total electrodes relatively lower because of the constraints of low active material proportion. Therefore, it is interesting to find new substrate materials to get rid of the constraints of the low loading of the active materials. The melamine foam (MF), a cellular structure with open cells,[18–20] has stimulated much interest because of its large pore size (100–150 μm) and the low bulk density (10.3 kg m^{-3}).[21] These features facilitate it to prepare composite materials including metal and nonmetals.

On the other hand, there is a considerable interest in conducting polymers because of their extensive potential applications in areas such as energy-storage and separations, catalysts, and chemical sensing. Among all of the conducting polymers, PPy has attracted

Additional Supporting Information may be found in the online version of this article.

considerable attention owing to its high electrical conductivity, the excellent stability for redox and the benign property to environment. As an excellent candidate for pseudo-capacitor electrodes, coating PPy on various substrates has been reported. For example, the PPy decorated on cellulose has been used in energy storage applications.[14] Liu et al. have deposited ultra-thin PPy layers on the highly conductive carbon substrate.[22] We have deposited the composite of PPy/MnO_2 on polypropylene fibrous membrane through a simple route of vapor polymerization.[15] In order to increase the C_{sc} of conducting polymers further, there have been many attempts to synthesize composite to compensate for the limitation of each individual material in electrochemical capacitors. Carbon nanotubes (CNTs) are considered to be a attracting material for composites.[23–27] Recently, composites of CNTs with metal oxides[25,28,29] and conducting polymers[26,30] have been synthesized and investigated. The results show that the presence of CNTs can improve the capacitive property due to its high conductivity. However, there are few literatures on the composite of PPy and MF used in electrical energy storage till now.

Here the composites deposited on the MF consisting of CNTs and PPy are prepared and used as the electrodes for supercapacitors. First, CNTs are loaded on the MF by dip-dry process, and then PPy is conveniently synthesized through a route of vapor polymerization *in situ*.[15] In order to improve the conductivity of the composites, CNTs are coated on the composite again by dip-dry process. Considering the structure of MF, it is expected that the composites will contain large ratio of active materials, and exhibit good flexibility.

EXPERIMENTAL

Reagents and Materials

Acetonitrile, anhydrous ethanol, anhydrous methanol, KCl, and $FeCl_3{\cdot}6H_2O$ were of analytical grade and used without further purification. Pyrrole (A.R., Shanghai Chemical Reagent) was purified through distillation under reduced pressure and stored at a temperature less than 5°C. The CNTs was obtained from department of chemical engineering of Tsinghua University and treated in mixed acid of H_2SO_4 and HNO_3.[31] The MF with a thickness of about 3.0 mm was purchased from company of Changzhou Yiteng rubber and plastic products.

Preparation of the Flexible Composites of PPy/CNTs/MF and CNTs/PPy/CNTs/MF

The slices of MF (10×31×3 mm, length×width×thickness) were used as substrates for the preparation of the composites. The original slices of MF were washed by anhydrous ethanol to remove the impurities. Then the slices of MF were immersed in the dispersion of CNTs (2 mg mL^{-1}), sometimes vacuum condition was used to help removing the air adsorbed in the MF. After the MF immersed completely in the solution for 3 min, they were taken out and dried at 80°C. To load different mass of CNTs, the above process could be repeated different times. The weight of CNTs loaded on the slices of MF was determined by using a precision balances. The samples of CNTs loaded on MF were defined as CNTs/MF.

The composite of PPy/CNTs/MF was prepared by using $FeCl_3{\cdot}6H_2O$ dissolved in acetonitrile as oxidant to react with the pyrrole vapor in an airtight vessel at room temperature. Briefly, the CNTs/MF were soaked in the $FeCl_3{\cdot}6H_2O$ solution of acetonitrile (50 mg mL^{-1}) for 5 min. After the excess solution was adsorbed by a filter paper, CNTs/MF containing $FeCl_3{\cdot}6H_2O$ solution was suspended in a sealed vessel where the oxidant reacted with the pyrrole vapor at room temperature for 24 h. Finally, the composite of PPy/CNTs/MF was dried at 80°C for 4 h after the impurity being removed through washing with ethanol and methanol for several times. Furthermore, the optimum PPy/CNTs/MF composite was immerged in the dispersion of CNTs (2.0 mg mL^{-1}) for 5 min, then it was taken out and dried at 80°C, finally the composite of CNTs/ PPy/CNTs/MF was obtained. In order to make a comparison, the PPy deposited on the MF without loading CNTs was also prepared and denoted as PPy/MF.

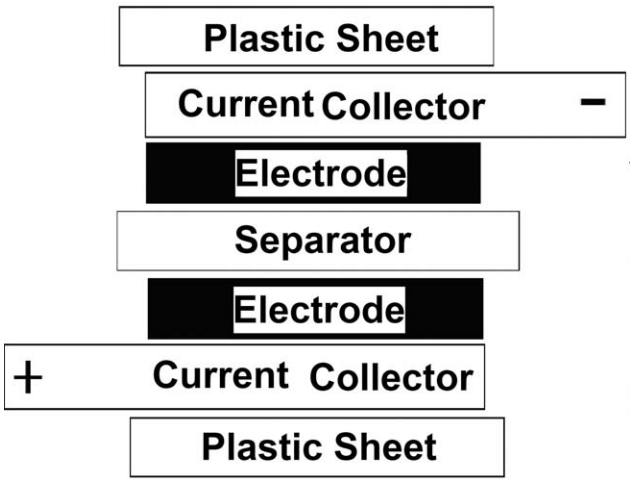

Figure 1. Construction of conventional test cell.

Characterization of Materials

The X-ray diffraction (XRD) patterns were recorded on a Bruker D8 Advance X-ray diffractometer (Cu Ka) in the 2θ range of 5–80° and the morphologies of the composites were observed on a scanning electron microscope (JEOL SEM 6701F). The resistances of the composites were measured by using a multimeter (Uni-trend Technology(China)), the mass of the CNTs and the PPy in the composites were measured by using a precision balance (Mettler Toledo weighing equipment system).

Electrochemical Measurements

Figure 1 shows the structural illustration of the capacitor cell assembled by the composites. The capacitor cells were assembled by using two same pieces of composites (one oxidized and the other reduced) as the two electrodes (the size of every composite is about 5×5 mm), and a piece of filter paper soaked with 1.0 mol L^{-1} KCl was used to separate the two pieces of composites. The electrochemical characteristics were evaluated using cyclic voltammetry (CV) and galvanostatic charge/discharge method. All the electrochemical performances were measured by using 1.0 mol L^{-1} KCl aqueous solution as electrolyte on a CHI 660C electrochemical station at room temperature. The C_{sc} of the electrodes was calculated based on the CV curves and the discharged current density ranging from 0.4

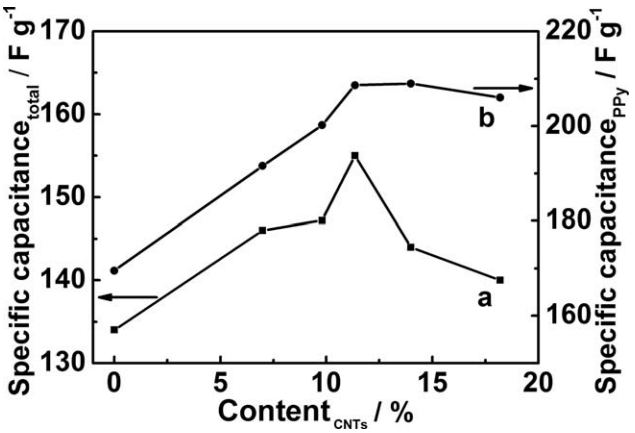

Figure 2. The relationships of specific capacitance (according to the mass of the active material and the total electrode) for PPy/CNTs/MF and the content of CNTs in the composite materials by CV at 1 mV s^{-1}.

to 1.0 A g^{-1}. The CV curves of the cell were recorded over the voltage range of −0.5 to 0.5 V at a scan rate from 1 to 20 mV s^{-1}. The electrochemical impedance spectra (EIS) were recorded at open-circuit potential in the frequency ranged from 10^5 to 10^{-2} Hz with ac-voltage amplitude of 5 mV.

RESULTS AND DISCUSSION

Characterization

The relationship between the values of C_{cs} and the content of CNTs is shown in Figure 2, it can be seen that the PPy/MF exhibits lower C_{cs} than that of all the samples of PPy/CNTs/MF, and that the value of C_{cs} based on PPy increases with increment of CNTs in samples of PPy/CNTs/MF. For example, when the content of CNTs in the composite reaches to about 11.3%, the value of C_{cs} reaches to the maximum (208.7 F g^{-1}), and almost maintains this level although the content of CNTs increases further [Figure 2(a)]. However, the values of C_{cs} based on the total mass of the composites exhibit a different trend. The value of C_{cs} increases with the increment of CNTs in the composites initially while decreases with the increase of CNTs content after the value of C_{cs} reaches to the maximum of 155 F g^{-1} at CNTs content of 11.3% [Figure 2(b)]. So the composites of PPy/CNTs/MF containing 11.3% CNTs are chosen in the following experiments.

Figure 3(A) shows the photographs of CNTs/PPy/CNTs/MF composite in the bending state, and it can be seen that the composite exhibits good flexibility. As displayed in Figure 3(B), it can be seen that the XRD patterns of PPy/CNTs/MF, CNTs/PPy/CNTs/MF show a diffraction peak at $2\theta = 26°$ which is ascribed to the (002) reflection of CNTs. The reflection of the chains of PPy can not be differentiated because the diffraction peak of it overlaps with CNTs in this region.[32] However, there are no peaks related to MF observed in the whole XRD patterns.

Scanning electron microscopy is used to reveal the microstructures of composite materials. As shown in Figure 4(A) (inserted figure), the SEM image of the CNTs/MF shows that the MF has kept a cellular structure with open cells and the surface of the fibers is coated with CNTs. From the SEM image of the composite of PPy/MF, it can be found that the open cells are almost occupied by the formed PPy with porous structure, and that the primary particles of PPy are large and the connection among the particles is loose [Figure 4(B)]. The SEM of PPy/CNTs/MF is presented in Figure 4(C), which is obviously different from that of CNTs/MF and PPy/MF. It shows that PPy has formed on the surface of fibers and in partial spaces of pores, and that the connection between the PPy particles is close because CNTs are wrapped in polypyrrole layer. The composite of CNTs/PPy/CNTs/MF [Figure 4(D)] shows a similar characteristic to PPy/CNTs/MF (inserted figure). Furthermore, from the magnified SEM image it can be found that a thin layer of CNTs has coated on the PPy, which will enhance the conductivity and improve the capacitive performance. The resistance of the samples of CNTs/MF decreases with the increment of CNTs content (Supporting Information). The resistances of the samples are measured by two-electrode and the resistivities were calculated to be about 3.45, 6.75, 2.4, and 0.75 Ω · m for CNTs/MF, PPy/MF, PPy/CNTs/MF, and CNTs/PPy/CNTs/MF, respectively.

Capacitive Properties of the Cells Assembled by PPy/CNTs/MF and CNTs/PPy/CNTs/MF

The CV curves at different scan rates for capacitor assembled by the PPy/CNTs/MF and CNTs/PPy/CNTs/MF are recorded and shown in Figure 5(A,B). It can be found that the curves at different scan rates do not show obvious redox peaks in the whole voltage range during the positive and negative sweeps, indicating that the electrode is charged and discharged at a pseudo-constant

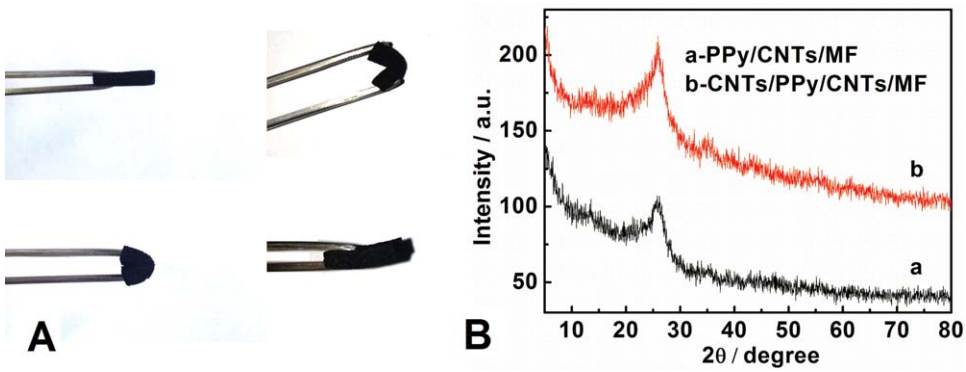

Figure 3. The photograph of the CNTs/PPy/CNTs/MF composite under bending condition (A).The XRD patterns of PPy/CNTs/MF and CNTs/PPy/CNTs/MF composites. [Color figure can be viewed in the online issue, which is available at wileyonlinelibrary.com.]

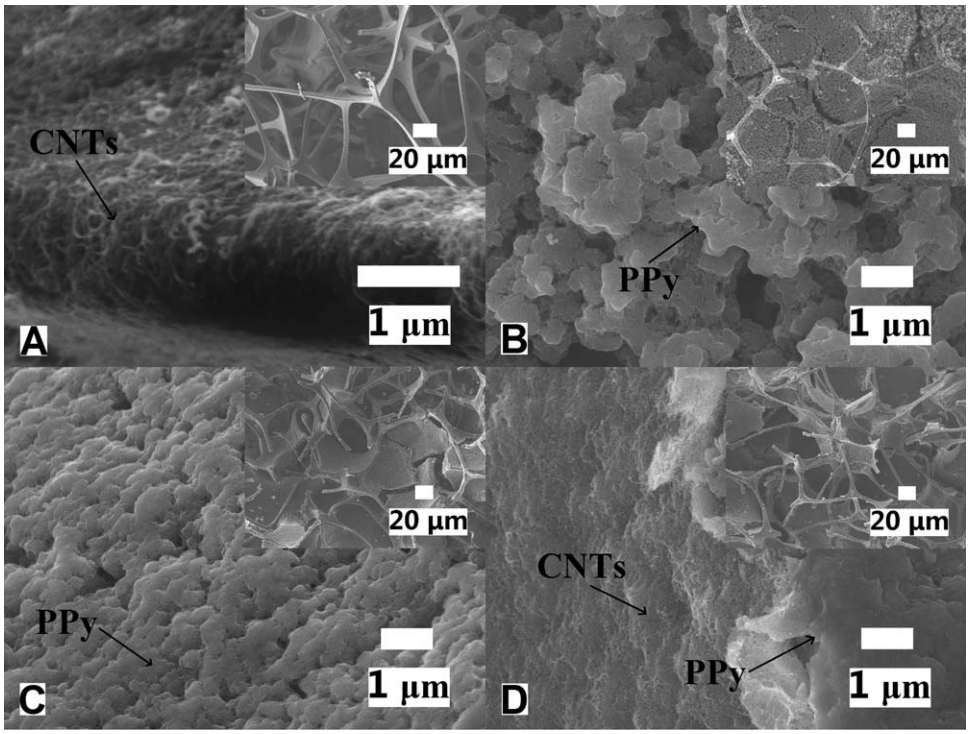

Figure 4. SEM images of (A) CNTs/MF, (B) PPy/MF, (C) PPy/CNTs/MF, (D) CNTs/PPy/CNTs/MF. The inserted figures are the SEM images in low magnification.

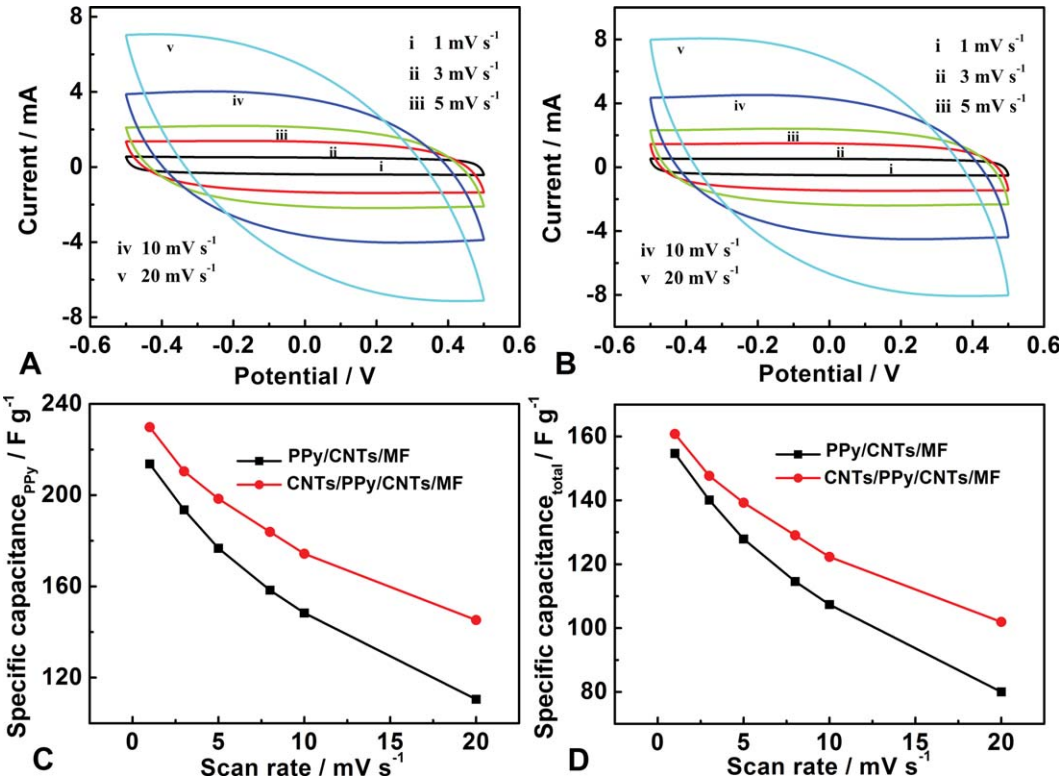

Figure 5. CV behaviors of the capacitor cells assembled by PPy/CNTs/MF (A), CNTs/PPy/CNTs/MF (B), (C) and (D) show the plots of specific capacitances of the capacitor cell prepared by PPy/CNTs/MF and CNTs/PPy/CNTs/MF. [Color figure can be viewed in the online issue, which is available at wileyonlinelibrary.com.]

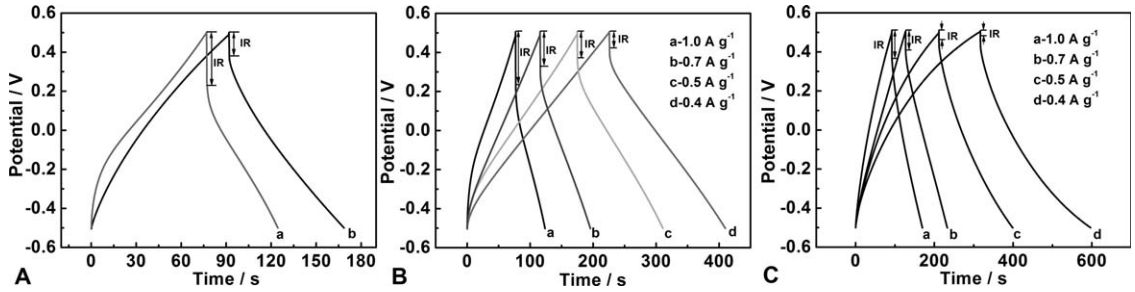

Figure 6. Charge/discharge curves of PPy/CNTs/MF(a) and CNTs/PPy/CNTs/MF(b) at current density of 1.0 A g^{-1} (A), charge/discharge curves of the cell assembled by PPy/CNTs/MF, CNTs/PPy/CNTs/MF at various current densities (B) and (C).

rate over the whole CV process. The shapes of the curves are rectangular-like with the almost symmetric *I-E* responses when the scan rates are lower than 10 mV s^{-1} [Figure 5(A-iv)]. It can be also found that the CV curves shown in Figure 5(B) display more rectangular-like than that shown in Figure 5(A), which illustrates that the composite of CNTs/PPy/CNTs/MF exhibits better capacitive property than composite of PPy/CNTs/MF.

It is well known that the redox reactions occurring on the PPy mainly attend by the doping-undoping counter ion (in this case Cl^-) in the matrix of the polymer,[33] and that the oxidation/reduction peaks of PPy can be observed when very thin PPy film deposited on the metallic electrodes is measured by using the three-electrode system. Furthermore, the oxidation/reduction peaks of PPy become very broad with the increase of the thickness of PPy due to the overpotential caused by the ions diffusion in the thick films. Usually, the properties of capacitor assembled by two pieces of PPy-based composite are tested by two-electrode system, one piece of composite is oxidized and the other is reduced during the test, which will make the oxidation/reduction peaks of PPy more unobvious and show the rectangular CV shape. At low scanning rates, the ions diffused from the electrolyte can access to almost all available spaces and lead to a complete insertion reaction, which will make a good rectangular CV shape. However, with the increase of the scanning rates, the effective interaction between the matrix and the electrolyte will reduce greatly due to the slow diffusion of ions in the matrix of polymer, so the deviation from rectangularity of the CV becomes obvious. The rectangular-like CV curves can only be observed at low scan rates, which indicate that the composites exhibit poor properties for quick charge and discharge. This mainly results from the large size of the formed PPy, which increases the difficulty for ion doping-undoping in the PPy matrix. However, the coating of CNTs on PPy surface increases the conductivity, which can partially compensate the defect caused by the large particles.

To analyze the variation of capacitance with varying scanning rate, the specificapacitance of the cell can be calculated based on CV curves according to equation:[34]

$$C_{sc}=(\int IdV)/(vm\Delta V) \quad (1)$$

where I is the response current (A), ΔV the difference of potential during the CV tests (V), υ the potential scan rate (V s^{-1}), and m the mass of the one electrode (g). Figure 5(C,D) shows the plots of the values of C_{sc} for the composites of PPy/CNTs/MF and CNTs/PPY/CNTs/MF versus scan rates ranging from 1 to 20 mV s^{-1}. It can be seen that the values of C_{sc} decrease gradually with the increment of the scan rate. Furthermore, it is found that the composite of CNTs/PPy/CNTs/MF exhibit larger C_{sc} (232 F g^{-1}) than that of composite PPy/CNTs/MF (205 F g^{-1}) based on the active materials. It is also proved that CNTs coating on PPy can improve the properties of the composites.

Figure 6(A) shows the charge/discharge curves of the cells prepared by PPy/CNTs/MF and CNTs/PPy/CNTs/MF at 1.0 A g^{-1}. The curve b shows longer discharge time than curve a, which indicates that CNTs/PPy/CNTs/MF has larger C_{sc} than PPy/CNTs/MF. Figure 6(B,C) shows the typical galvanostatic charge/discharge curves of the cells assembled by PPy/CNTs/MF and CNTs/PPy/CNTs/MF at current densities of 0.4, 0.5, 0.7, and 1.0 A g^{-1}, it is found that the charging curves are almost symmetric to their discharging counterparts in the whole potential region. It can also be found from Figure 6(B,C) that the *IR* drops increase with the increase of the discharged current densities, and that the discharge times are longer and *IR* drops are smaller in Figure 6(C) than that in Figure 6(B) at the same discharged current density.

The C_{sc} can also be calculated according to the discharged curves by using the equations:

$$C_{sc}=2(I\Delta t/m\Delta V) \quad (2)$$

where I is the constant discharge current, Δt the discharging time, m the mass of active material (when calculating the C_{sc} of total electrode, m is the quality of one electrode), and ΔV the potential window. From the plots of C_{sc} versus the discharged current density shown in Figure 7, it can be seen that the C_{sc} decreases when the discharge current increases for all the cells assembled by the composites, but the composite of CNTs/PPy/CNTs/MF shows larger C_{sc} (262 F g^{-1}) than that of PPy/CNTs/MF (167 F g^{-1}) and exhibit slighter trend of decrement than that of PPy/CNTs/MF according to the active materials. Recently, Kim et al.[35] have deposited the thin film of PPy on platinum electrode and found that the C_{sc} of PPy can reach to 380 F g^{-1}. Bose et al.[36] have fabricated the graphene-PPy nanocomposite with a C_{sc} value of 267 F g^{-1} at 100 mV s^{-1}. Compared with the similar storage devices which have reported, it is found that our composites exhibit the moderate value of C_{sc} based on the active material due to the low conductivity of the substrates and the large particles of PPy.

The repeated galvanostatic charge/discharge curves of the cells assembled by PPy/CNTs/MF and CNTs/PPy/CNTs/MF at current density of 0.5 A g^{-1} are shown in Figure 8, it is found that

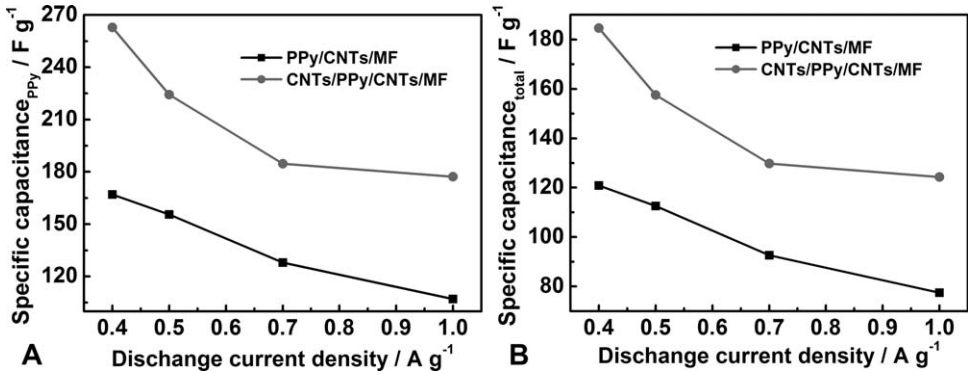

Figure 7. Discharge capacitance of the capacitors assembled by PPy/CNTs/MF and CNTs/PPy/CNTs/MF at various discharge current densities.

the cells assembled by CNTs/PPy/CNTs/MF exhibit better stability and smaller *IR* drop compared with PPy/CNTs/MF.

EIS can provide the electronic/ionic conductivity of the electrode materials during the charging/discharging progress. All the spectra are expected to exhibit a semicircle in the high-frequency region and a linear portion at low-frequency region. The interception of the semicircle at the real axis in the high frequency region represents the internal resistance related to the intrinsic electrical resistance of the active materials since the conditions of measurement are kept the same.[37] The Nyquist plots representing the imaginary part of the impedance and the real part of the composites are shown in Figure 9(A). The single semicircle in the high-frequency region and a straight line in the low-frequency region are observed. From the inserted plots, it is found that the charge-transfer resistance of the cell assembled by CNTs/PPy/CNTs/MF is smaller than that assembled by PPy/CNTs/MF, which is an important factor in the electrochemical capacitor.[38] This also indicates that the out layer of CNTs in CNTs/PPy/CNTs/MF has improved the conductivity and makes the composite having better electrochemical capacity compared with PPy/CNTs/MF. The cyclic stability of the cells is one of the important factors for their practical application. As shown in Figure 9(B), the value of C_{sc} of PPy/

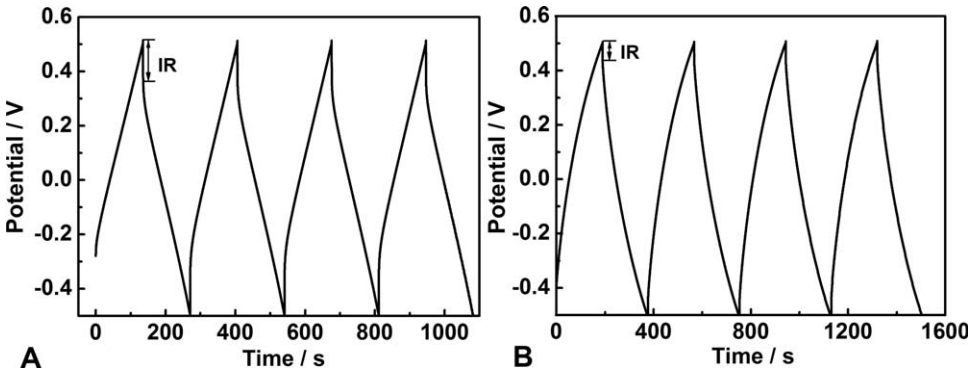

Figure 8. Charge/discharge cycling curves of the cells prepared by PPy/CNTs/MF (A), CNTs/PPy/CNTs/MF(B) at current density of 0.5 A g^{-1}.

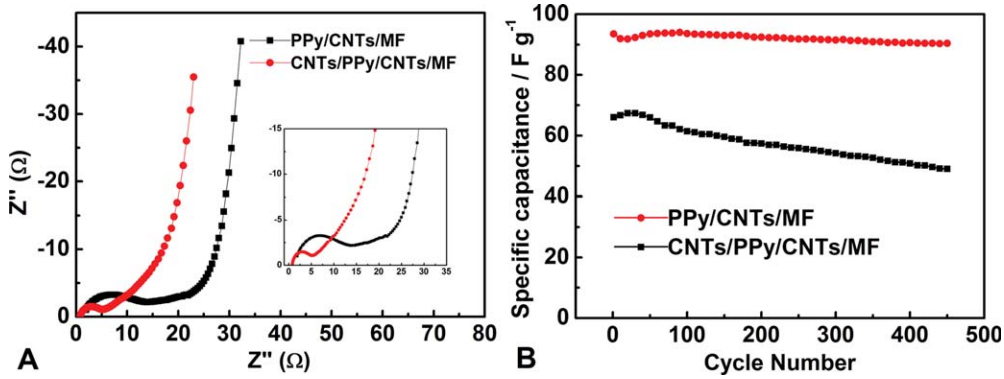

Figure 9. Nyquist plots of the capacitors assembled by PPy/CNTs/MF and CNTs/PPy/CNTs/MF (insert is the EIS in high-frequency region) (A). the relationships between the specific capacitance of the cells and the cycle numbers under successive CV scan at 20 mV s^{-1}(B). [Color figure can be viewed in the online issue, which is available at wileyonlinelibrary.com.]

CNTs/MF decreases 27% of the initial capacity at 20 mV s^{-1} after 450 cycles. However, the capacity loss of the cell assembled by CNTs/PPy/CNTs/MF is only 3.8% after 450 cycles, confirming the excellent cyclic stability of the CNTs/PPy/CNTs/MF electrode and may be developed as a suitable material for electrochemical capacitors applications.

CONCLUSIONS

We have fabricated the composites of PPy/CNTs/MF and CNTs/PPy/CNTs/MF by combining the dip-dry process and chemical polymerization in vapor phase. The obtained composites are lightweight, flexible and mechanically robust. The C_{sc} based on the PPy mass and the total mass of the electrodes are about 262 and 184 F g^{-1} for CNTs/PPy/CNTs/MF composite, which are higher than that for the PPy/CNTs/MF (167 and 129 F g^{-1}) at the discharge current of 0.4 A g^{-1}. In addition, the free-standing CNTs/PPy/CNTs/FM has excellent cyclic stability. According to the above results, such CNTs/PPy/CNTs/MF is very promising for flexible energy storage devices. The properties of the composites for quick charge/discharge may be improved by making the conductive materials (CNTs, graphene and so on) not only coated on the fibers of MF but also filled in the pores to form continuous microstructure.

ACKNOWLEDGMENTS

The authors thank the National Natural Science Foundation of China (21274082 and 21073115) and Shanxi province (2012021021-3), the Program for New Century Excellent Talents in University (NCET-10-0926) of China and the Program for the Top Young and Middle-aged Innovative Talents of Shanxi province (TYMIT), and the returned personnel of scientific research project of Shanxi (2011-003).

REFERENCES

1. Sun, Y.; Rogers, J. A. *Adv. Mater.* **2007**, *19*, 1897.
2. Kaltenbrunner, M.; Kettlgruber, G.; Siket, C.; Schwödiauer, R.; Bauer, S. *Adv. Mater.* **2010**, *22*, 2065.
3. Hu, L. B.; Pasta, M.; Mantia, L. F.; Cui, L. F.; Jeong, S.; Deshazer, H. D.; Choi J. W.; Han, S. M.; Cui, Y. *Nano Lett.* **2010**, *10*, 708.
4. Kaltenbrunner, M.; White, M. S.; Glowacki, E. D.; Sekitani, T.; Someya, T.; Sariciftci, N. S.; Bauer, S. *Nat. Commun.* **2012**, *3*, 770 doi: 10.1038/ncomms 1722.
5. Hiralal, P.; Imaizumi, S.; Unalan, H. E.; Matsumoto, H.; Minagawa, M.; Rouvala, M.; Tanioka, A.; Amaratunga, G. A. J. *ACS Nano* **2010**, *4*, 2730.
6. Nam, K. T.; Kim, D. W.; Yoo, P. J.; Chiang, C. Y.; Meethong, N.; Hammond, P. T.; Chiang, Y. M.; Belcher, A. M. *Science* **2006**, *312*, 885.
7. Chen, J.; Liu, Y.; Minett, A. I.; Lynam, C.; Wang, J. Z.; Wallace, G. G. *Chem. Mater.* **2007**, *19*, 3595.
8. Hu, S.; Rajamani, R.; Yu, X. *Appl. Phys. Lett.* **2012**, *100*, 103.
9. Kaempgen, M.; Chan, C. K.; Ma, J.; Cui, Y.; Gruner, G. *Nano Lett.* **2009**, *9*, 1872.
10. Cheng, Q.; Tang, J.; Ma, J.; Zhang, H.; Shinya, N.; Qin, L. C. *J. Phys. Chem. C* **2011**, *115*, 23584.
11. Winter, M.; Brodd, R. J. *Chem. Rev.* **2004**, *104*, 4245.
12. Miller, J. R.; Simon, P. *Science* **2008**, *321*, 651.
13. Simon, P.; Gogotsi, Y. *Nat. Mater.* **2008**, *7*, 845.
14. Kim, S. Y.; Hong, J. K.; Palmore, G. T. R. *Synth. Met.* **2012**, *162*, 1478.
15. Jin, M.; Han, G. Y.; Chang, Y. Z.; Zhao, H.; Zhang. H. Y. *Electrochim. Acta* **2011**, *56*, 9838.
16. Wu, Q.; Xu, Y. X.; Yao, Z. Y.; Liu, A. R.; Shi, G. Q. *ACS Nano* **2010**, *4*, 1963.
17. Lee, H.; Kim, H.; Cho, M. S.; Choi, J.; Lee. Y. *Electrochim. Acta* **2011**, *56*, 7460.
18. Wang, Y. B.; Sotzing, G. A.; Weiss, R. A. *Polymer* **2006**, *47*, 2728.
19. Magnenet, V.; Rahouadj, R.; Bacher, P.; Cunat, C. *Mech. Mater.* **2008**, *40*, 673.
20. Price, D.; Liu, Y.; Milnes, G. J.; Hull, R.; Kandola, B. K.; Horrocks, A. R. *Fire Mater.* **2002**, *26*, 201.
21. Kino, N.; Ueno, T. *Appl. Acoust.* **2008**, *69*, 325.
22. Kim, J. H.; Lee, Y. S.; Sharma, A. K.; Liu, C. G. *Electrochim. Acta* **2006**, *52*, 1727.
23. Lota, G.; Fic, K.; Frackowiak, E. *Energy Environ. Sci.* **2011**, *4*, 1592.
24. Fang, W. C.; Chyan, O.; Sun, C. L.; Wu, C. T.; Chen, C. P.; Chen, K. H.; Chen, L. C.; Huang, J. H. *Electrochem. Commun.* **2007**, *9*, 239.
25. Zhang, H.; Cao, G. P.; Wang, Z. Y.; Yang, Y. S.; Shi, Z. j.; Gu, Z. N. *Nano Lett.* **2008**, *8*, 2664.
26. Meng, C. Z.; Liu, C. H.; Fan, S. S. *Electrochem. Commun.* **2009**, *11*, 186.
27. Lee, H.; Cho, M. S.; Kim, I. H.; Nam, J. D.; Lee, Y. *Synth. Met.* **2010**, *160*, 1055.
28. Li, J.; Yang, Q. M.; Zhitomirsky, I. *J. Power Sources* **2008**, *185*, 1569.
29. Chou, S. L.; Wang, J. Z.; Chew, S. Y.; Liu, H. K.; Dou, S. X. *Electrochem. Commun.* **2008**, *10*, 1724.
30. Zhang, H.; Cao, G. P.; Wang, Z. Y.; Yang, Y. S.; Shi, Z. J.; Gu, Z. N. *Electrochem. Commun.* **2008**, *10*, 1056.
31. Han, G. Y.; Yuan, J. Y.; Shi, G. Q.; Wei, F. *Thin Solid Films* **2005**, *474*, 64.
32. Lu, X. J.; Dou, H.; Yuan, C. Z.; Yang, S. D.; Hao, L.; Zhang, F.; Shen, L. F.; Zhang, L. J.; Zhang, X. G. *J. Power Sources.* **2012**, *197*, 319.
33. Huang, L. M.; Wen, T. C.; Gopalan, A. *Electrochim. Acta.* **2006**, *5*, 3469.
34. Fan, Z. J.; Yan, J.; Wei, T.; Zhi, L. J.; Ning, G. Q.; Li, T. Y.; Wei, F. *Adv. Funct. Mater.* **2011**, *21*, 2366.
35. Kim, B. C.; Too, C. O.; Kwon, J. S.; Ko, J. M.; Wallace, G. G. *Synth. Met.* **2011**, *161*, 1130.
36. Bose, S.; Kim, N. H.; Kuila, T.; Lau, K. T.; Lee, J. H. *Nanotechnology* **2011**, *22*, 295202(1-9).
37. Kim, D. W.; Noh, K. A.; Chun, J. H.; Kim, S. H.; Ko, J. M. *Solid State Ionics* **2001**, *144*, 329.
38. Bakhmatyuk, B. P.; Venhryn, B. Y.; Grygorchak, I. I.; Micov, M. M. *J. Power Sources* **2008**, *180*, 890.